Supporting Information

Wing and Halevy 10.1073/pnas.1407502111

SI Materials and Methods

Multireactant, Multiproduct Enzymatic Reactions. The net flux through a single, reversible, enzymatically catalyzed step in a metabolic pathway can be expressed as (1)

$$J = J^+ - J^- = [E] \times k_{\text{cat}}^+ \times \left(\frac{\prod_j \left([r_j]/K_{Mj} \right)^{n_j}}{1 + \prod_j \left([r_j]/K_{Mj} \right)^{n_j} + \prod_i \left([p_i]/K_{Mi} \right)^{m_i}} \right) \times \left(1 - e^{\Delta G_r / RT} \right), \quad \textbf{[S1]}$$

where J is the net flux, and J^+ and J^- are the forward and reverse fluxes, respectively. $[E]$ is enzyme concentration, k_{cat}^+ is the forward catalytic rate constant, $[r_j]$ is the concentration of reactant j, K_{Mj} is the half-saturation constant of reactant j for the enzyme, and n_j is the stoichiometry of the reactant in the reaction. Likewise, $[p_i]$ is the concentration of product i, K_{Mi} is the half-saturation constant of product i for the enzyme, and m_i is the stoichiometry of the product in the reaction. ΔG_r is the Gibbs free energy of the reaction, R is the gas constant, and T is the temperature.

In what follows, we replace the term $[E] \times k_{\text{cat}}^+$ with a maximal metabolic rate capacity, V^+. For brevity in derivation of the rate equations for the specific reactions in the sulfate reduction pathway, we further omit the subscripts M from the half-saturation constants and the subscript r from the Gibbs free energy of reaction:

$$J = V^+ \left(\frac{\prod_j \left([r_j]/K_j \right)^{n_j}}{1 + \prod_j \left([r_j]/K_j \right)^{n_j} + \prod_i \left([p_i]/K_i \right)^{m_i}} \right) \left(1 - e^{\Delta G / RT} \right). \quad \textbf{[S2]}$$

The first term on the right-hand side of Eq. **S2** ("kinetic term") relates the forward flux to the reverse flux through the dependence on enzyme kinetics, whereas the second term ("thermodynamic term") relates these fluxes through the thermodynamic driving force or the departure from thermodynamic equilibrium. In its simplified form, Eq. **S2** is exactly equivalent to Eq. **4** in the main text.

Isotopic Fractionation in Linear, Reversible Metabolic Reaction Networks. Starting with the final pool (p) in the general reaction network,

$$t \underset{\phi_{st}}{\overset{\phi_{ts}}{\rightleftharpoons}} s \underset{\phi_{rs}}{\overset{\phi_{sr}}{\rightleftharpoons}} r \underset{\phi_{pr}}{\overset{\phi_{rp}}{\rightleftharpoons}} p,$$

where t, s, r, and p are metabolite pools, and ϕ_{rp}, for example, is the flux between pools r and p, we express the net flux of mass and isotopes,

$$\phi_{\text{net}} = \phi_{rp} - \phi_{pr}, \quad \textbf{[S3]}$$

$$\phi_{\text{net}} R_p = \phi_{rp} R_{rp} - \phi_{pr} R_{pr}, \quad \textbf{[S4]}$$

where R_p, R_{rp}, and R_{pr} are the $^{34}S/^{32}S$ (or $^{33}S/^{32}S$) ratios of p and the fluxes ϕ_{rp} and ϕ_{pr}, respectively. Noting that the isotopic fractionation factor between any two pools a and b is $\alpha_{a,b} \equiv R_a/R_b$, and substituting the expression for ϕ_{net} from Eq. **S3** into Eq. **S4**, we obtain

$$\left(\phi_{rp} - \phi_{pr} \right) R_p = \phi_{rp} \alpha_{rp,r} R_r - \phi_{pr} \alpha_{pr,p} R_p. \quad \textbf{[S5]}$$

Here $\alpha_{rp,r}$, the isotopic fractionation between the flux ϕ_{rp} and the pool r, is by definition the kinetic fractionation associated with transformation from pool r to pool p. Rearranging to solve for R_r/R_p yields

$$\frac{R_r}{R_p} = \frac{\phi_{rp} - \phi_{pr} + \phi_{pr} \alpha_{pr,p}}{\phi_{rp} \alpha_{rp,r}}. \quad \textbf{[S6]}$$

We express the equilibrium fractionation factor between pools r and p, $\alpha_{r,p}^{\text{eq}}$, by considering the isotopic mass balance at equilibrium, $\phi_{rp} \alpha_{rp,r} R_r = \phi_{pr} \alpha_{pr,p} R_p$ (2), which yields $R_r/R_p = \alpha_{r,p}^{\text{eq}} = \alpha_{pr,p}/\alpha_{rp,r}$. Defining $f_{p,r} \equiv \phi_{pr}/\phi_{rp}$ to be the ratio of the reverse to forward flux, we obtain

$$\frac{R_r}{R_p} = \frac{1}{\alpha_{rp,r}} - \frac{f_{p,r}}{\alpha_{rp,r}} + f_{p,r} \alpha_{r,p}^{\text{eq}} = \alpha_{r,rp} + f_{p,r} \left(\alpha_{r,p}^{\text{eq}} - \alpha_{r,rp} \right). \quad \textbf{[S7]}$$

This expression for the fractionation factor between pools r and p is a function of the equilibrium fractionation factor, the kinetic fractionation associated with the reaction, and the ratio of the reverse to forward rate, $f_{p,r}$:

$$\boldsymbol{\alpha_{r,p}} = \left(\alpha_{r,p}^{\text{eq}} - \alpha_{r,rp} \right) \times f_{p,r} + \alpha_{r,rp}. \quad \textbf{[S8]}$$

This expression for the fractionation factor naturally yields the equilibrium fractionation factor when $\phi_{rp} = \phi_{pr}$ (i.e., when $f_{p,r} = 1$) and the kinetic fractionation factor when $\phi_{rp} \gg \phi_{pr}$ (i.e., when $f_{p,r} \to 0$). It is exactly equivalent to Eq. **1** in the main text.

Constructing a similar mass budget for the reaction between pools s and r under the assumption of a steady state ($\phi_{\text{net}} = \phi_{rp} - \phi_{pr} = \phi_{sr} - \phi_{rs}$) and recalling that $R_r = \boldsymbol{\alpha_{r,p}} R_p$, we ultimately obtain a recursive expression for the fractionation between pools s and p:

$$\boldsymbol{\alpha_{s,p}} = \left(\alpha_{s,r}^{\text{eq}} \times \boldsymbol{\alpha_{r,p}} - \alpha_{s,sr}\right) \times f_{r,s} + \alpha_{s,sr}. \quad \textbf{[S9]}$$

That is, near equilibrium ($\phi_{sr} = \phi_{rs}$ or $f_{r,s} = 1$), the fractionation associated with the combination of the two reactions between s and r, and between r and p, is the product of the equilibrium fractionation factor of the upstream step ($\alpha_{s,r}^{\text{eq}}$) and the fractionation inherited from the downstream step ($\boldsymbol{\alpha_{r,p}}$). Far from equilibrium ($\phi_{sr} \gg \phi_{rs}$ or $f_{r,s} \to 0$), memory of the fractionation inherited from the downstream reaction is lost, and the fractionation factor is simply the kinetic fractionation factor associated with the reaction of pool s to form pool r.

Expanding this treatment to include also the reaction between pools t and s, we obtain a recursive expression for the fractionation between the initial reactant (t) and the final product (p):

$$\boldsymbol{\alpha_{t,p}} = \left(\alpha_{t,s}^{\text{eq}} \times \boldsymbol{\alpha_{s,p}} - \alpha_{t,ts}\right) \times f_{s,t} + \alpha_{t,ts}. \quad \textbf{[S10]}$$

This can be expanded to treat any linear network consisting an arbitrary number of reversible reactions. It then remains to obtain expressions for the ratios of the reverse to forward fluxes (which we hereafter generalize as $f_{p,r}$). This is done by dividing both sides of Eq. **S1** by the forward flux, J^+, and rearranging to get

$$f_{p,r} = e^{\Delta G/RT}. \quad \textbf{[S11]}$$

Because $\Delta G = \Delta G^o + RT \ln(\prod_i [p_i]^{m_i} / \prod_j [r_j]^{n_j})$, the value of $f_{p,r}$ is related to the energetics of the reaction at the standard state, the temperature, and the metabolite concentrations:

$$f_{p,r} = \frac{\prod_i [p_i]^{m_i}}{\prod_j [r_j]^{n_j}} e^{\Delta G^o/RT}. \quad \textbf{[S12]}$$

Relating Sulfate Reduction Rate to Sulfur Isotope Fractionation. The reactions in the metabolic pathway for dissimilatory sulfate reduction (Fig. 1 in main text) are shown in Table S1. Two assumptions are implicit in this list of reactions. First, free sulfur compounds of intermediate oxidation state (e.g., thiosulfate, zero-valent sulfur) are assumed not to play a role in setting S-isotope fractionations. The ability of the model to reproduce essentially all available experimental results lends confidence that this choice is not misguided. Second, menaquinone is assumed to be the ultimate electron carrier used by sulfate reducers during respiration. This second choice is justified by measurements of intracellular metabolite concentrations showing that menaquinone is by far the most abundant electron carrier in sulfate reducers (3). We note that recent work, however, has discussed alternative conceptual hypotheses in which both of these assumptions are released (4). The framework presented here could be used to quantitatively evaluate these hypotheses.

Following conventional approaches to biochemical thermodynamics for reactions occurring at a constant, specific pH (5), we calculate values of the transformed Gibbs free energy, $\Delta G^{o'}$, for reactions *B–D* at pH 7 and an ionic strength of 0.25, which are reasonable cytoplasmic values. For this purpose we use an online tool for biochemical thermodynamic analysis (http://equilibrator.weizmann.ac.il) (6). Reduced menaquinone and oxidized menaquinone were not included in this database. Therefore, we convert the $\Delta G^{o'}$ of APS reduction and sulfite reduction, using $FAD/FADH_2$ as the electron carriers, which is included in the database, into the $\Delta G^{o'}$ of these reactions with menaquinone as the electron carrier, using the redox potentials of $FAD/FADH_2$ and menaquinone(ox)/menaquinone (red) reported in ref. 7.

We calculate the Gibbs free energy (untransformed), ΔG^o, of reaction *A* (sulfate uptake), using the results of sulfate uptake experiments in *Desulfobulbus propionicus*, which transport sulfate actively into the cell along with H^+ ions to maintain charge balance (8). In these experiments, the dependence of intracellular sulfate concentrations ($[SO_4^{2-}]_{\text{in}}$) and the number of protons transported together with sulfate (n) on extracellular sulfate concentrations ($[SO_4^{2-}]_{\text{out}}$) was recorded. The proton-motive force (PMF) was also recorded in the experiments and found to be approximately constant with a value of -132×10^{-3} V. Using the measured values, we calculate the membrane potential ($\Delta\psi$ in V) and ΔG_A^o,

$$\Delta\psi = \frac{n \times \text{PMF}}{2} + \log\left(\frac{[SO_4^{2-}]_{\text{in}}}{[SO_4^{2-}]_{\text{out}}}\right)\frac{z}{2}, \quad \textbf{[S13]}$$

$$\Delta G_A^o = \frac{\Delta\psi(n-2)RT}{z}, \quad \textbf{[S14]}$$

where $z = 2.3RT/F$, R is the gas constant, T is the temperature, and F is Faraday's constant. The value of z is ~59 mV at 25 °C. The dependence of ΔG_A^o on extracellular sulfate concentrations is shown in Fig. S1. In addition, using the membrane potential calculated above, we calculate the ratio of internal to external $[H^+]$ indicated by the experimental results:

$$\frac{[H^+]_{in}}{[H^+]_{out}} = 10^{(PMF-\Delta\psi)/z}. \quad \textbf{[S15]}$$

We describe the rate of steps *A*–*D* in the sulfate reduction pathway with expressions in the form of Eq. **S2**:

$$J_A = V_A^+\left(\frac{[SO_4^{2-}]_{out}/K_{As1}}{1+[SO_4^{2-}]_{out}/K_{As1}+[SO_4^{2-}]_{in}/K_{Ap1}}\right)\times\left(1-\frac{[SO_4^{2-}]_{in}[H^+]_{in}^n}{[SO_4^{2-}]_{out}[H^+]_{out}^n}e^{\Delta G_A^o/RT}\right), \quad \textbf{[S16]}$$

$$J_B = V_B^+\left(\frac{[SO_4^{2-}]_{in}[ATP]/(K_{Bs1}K_{Bs2})}{1+[SO_4^{2-}]_{in}[ATP]/(K_{Bs1}K_{Bs2})+[APS][PPi]/(K_{Bp1}K_{Bp2})}\right)\times\left(1-\frac{[APS][PPi]}{[SO_4^{2-}]_{in}[ATP]}e^{\Delta G_B^{o'}/RT}\right), \quad \textbf{[S17]}$$

$$J_C = V_C^+\left(\frac{[APS][MK_{red}]/(K_{Cs1}K_{Cs2})}{1+[APS][MK_{red}]/(K_{Cs1}K_{Cs2})+[SO_3^{2-}][MK_{ox}][AMP]/(K_{Cp1}K_{Cp2}K_{Cp3})}\right)\times\left(1-\frac{[SO_3^{2-}][MK_{ox}][AMP]}{[APS][MK_{red}]}e^{\Delta G_C^{o'}/RT}\right), \quad \textbf{[S18]}$$

$$J_D = V_D^+\left(\frac{[SO_3^{2-}][MK_{red}]^3/(K_{Ds1}K_{Ds2}^3)}{1+[SO_3^{2-}][MK_{red}]^3/(K_{Ds1}K_{Ds2}^3)+[H_2S][MK_{ox}]^3/(K_{Dp1}K_{Dp2}^3)}\right)\times\left(1-\frac{[H_2S][MK_{ox}]^3}{[SO_3^{2-}][MK_{red}]^3}e^{\Delta G_D^{o'}/RT}\right). \quad \textbf{[S19]}$$

The subscripts *A*, *B*, *C*, and *D* denote the reactions in Table S1. The subscripts *s*1 and *s*2 denote the first and second substrates in the reaction, whereas *p*1–*p*3 denote the products. Note that the second parentheses in the right-hand sides of Eqs. **S16–S19** are simply $(1-f_{p,r})$ for the reactions. We assume that the experimental determinations of enzyme activities were conducted at pH values similar to those of the cell interior and do not require modification to account for pH differences. Additionally, $[H^+]$ does not appear in the thermodynamic term of reaction *D* because we use the transformed Gibbs free energy, following common biochemical thermodynamics approaches (5). This approach also requires that all calculations are performed in units of mols L^{-1} (5).

Measurements of enzyme activity of crude cell extracts of pure cultures provide a basis for estimating V^+. To account for differences between these in vivo enzyme activities and those measured in vitro in the crude extract experiments ($V^+_{\text{in vitro}}$; Table S2), we scaled the in vitro activity measurements of the various reaction steps. This scaling factor $u_{\text{vivo–vitro}}$ is defined as

$$u_{\text{vivo–vitro}} = \frac{[E]_{\text{in vivo}}\times k^+_{\text{cat,in vivo}}}{[E]_{\text{in vitro}}\times k^+_{\text{cat,in vitro}}}. \quad \textbf{[S20]}$$

Although specific activity may be affected by enzyme isolation and purification (9), we used experimental data from crude cell extracts to minimize this effect. As a result, we assume that enzyme structure remains constant in the in vivo and in vitro experiments and $k^+_{\text{cat,in vivo}} \approx k^+_{\text{cat, in vitro}}$. This means that the "vivo–vitro" scaling factor reduces to a measure of the relative concentration of active enzymes in whole cells vs. crude extracts,

$$u_{\text{vivo–vitro}} \approx \frac{[E]_{\text{in vivo}}}{[E]_{\text{in vitro}}}. \quad \textbf{[S21]}$$

Given the regulation of respiratory gene transcription by the same regulon in many sulfate reducers (10), we scaled all values of $V^+_{\text{in vitro}}$ (Table S2) by the same $u_{\text{vivo–vitro}}$, resulting in in vivo V^+ values for each step in the sulfate reduction pathway. The procedure we used to calibrate $u_{\text{vivo–vitro}}$ is explained below.

By definition, at a steady state, $J_A = J_B = J_C = J_D \equiv \mathbb{J}$, the overall rate of sulfate reduction. Under this constraint, we rearrange Eqs. **S16–S19** to solve for the intracellular concentrations of SO_4^{2-}, APS, PPi, and SO_3^{2-}:

$$[SO_4^{2-}]_{in} = \frac{\left[[SO_4^{2-}]_{out}/K_{As1} - (\mathbb{J}/V_A^+)(1+[SO_4^{2-}]_{out}/K_{As1})\right]}{\left[\mathbb{J}/V_A^+K_{Ap1} + ([H^+]_{in}/[H^+]_{out})^n(e^{\Delta G_A^o/RT}/K_{As1})\right]}, \quad \textbf{[S22]}$$

$$[APS] = \frac{\left[(\mathbb{J}/V_C^+)K_{Cs1}K_{Cs2}\times(1+[SO_3^{2-}][MK_{ox}][AMP]/(K_{Cp1}K_{Cp2}K_{Cp3})) + [SO_3^{2-}][MK_{ox}][AMP]e^{\Delta G_C^{o'}/RT}\right]}{\left[[MK_{red}](1-\mathbb{J}/V_C^+)\right]}, \quad \textbf{[S23]}$$

$$[PPi] = \frac{\left[[SO_4^{2-}]_{in}[ATP](1-\mathbb{J}/V_B^+) - (\mathbb{J}/V_B^+)K_{Bs1}K_{Bs2}\right]}{[APS]\left[(\mathbb{J}/V_B^+)(K_{Bs1}K_{Bs2}/(K_{Bp1}K_{Bp2})) + e^{\Delta G_B^{o'}/RT}\right]}, \quad \textbf{[S24]}$$

$$[SO_3^{2-}] = \frac{\left[(\mathbb{J}/V_D^+)K_{Ds1}K_{Ds2}^3\times\left(1+[H_2S][MK_{ox}]^3/(K_{Dp1}K_{Dp2}^3)\right) + [H_2S][MK_{ox}]^3e^{\Delta G_D^{o'}/RT}\right]}{\left[[MK_{red}]^3(1-\mathbb{J}/V_D^+)\right]}. \quad \textbf{[S25]}$$

Net sulfate reduction implies $\mathbb{J} > 0$, whereas the requirement for nonnegative intracellular metabolite concentrations places an upper limit on $\mathbb{J}$ (a requirement that the numerators and denominators of Eqs. **S22–S25** have the same sign). Once the equations are solved for the intracellular metabolite concentrations, we calculate the free energy for each of the reactions in the network:

$$\Delta G_A = \Delta G_A^o + RT \ln\left(\frac{[SO_4^{2-}]_{in}[H^+]_{in}^n}{[SO_4^{2-}]_{out}[H^+]_{out}^n}\right), \quad \textbf{[S26]}$$

$$\Delta G_B = \Delta G'^{o'}_B + RT \ln\left(\frac{[APS][PPi]}{[SO_4^{2-}]_{in}[ATP]}\right), \quad \textbf{[S27]}$$

$$\Delta G_C = \Delta G'^{o'}_C + RT \ln\left(\frac{[SO_3^{2-}][AMP][MK_{ox}]}{[APS][MK_{red}]}\right), \quad \textbf{[S28]}$$

$$\Delta G_D = \Delta G'^{o'}_D + RT \ln\left(\frac{[H_2S][MK_{ox}]^3}{[SO_3^{2-}][MK_{red}]^3}\right). \quad \textbf{[S29]}$$

We then use these values of the free energy to calculate the ratio of reverse to forward reaction rates ($f_{p,r}$), as in Eq. **S12**, and from these the fractionation between the initial substrate sulfate and ultimate product sulfide, using recursive expressions in the form of Eq. **S10**.

Model Calibration. The model parameters, required for solving Eqs. **S22–S25**, are listed in Tables S1–S4 along with constraints on their values, where such constraints exist. Six parameters, to which the model results are sensitive, remain truly variable ($[SO_4^{2-}]_{out}$, $[H_2S]_{in}$), poorly constrained ($^{34}\alpha_A^{kin}$, $^{34}\lambda_A^{kin}$), or both ($[MK_{red}]/[MK_{ox}]$, $u_{vivo-vitro}$). To calibrate the model we use a combination of constraints on physiologically possible intracellular metabolite concentrations and experimental $[SO_4^{2-}]_{out}$–csSRR–$^{34}\varepsilon$–$^{33}\lambda$ data.

Metabolomic compilations suggest that the majority of metabolite concentrations are less than 10 mM (11). Accordingly, we assume that the concentrations of all metabolites except sulfate are less than 10 mM. In addition, cell volume places a hard lower limit on metabolite concentrations from the requirement that at least one molecule of free metabolite exists in the cell. For a cell volume of ~1 μL, typical of sulfate reducers, this hard lower limit on metabolite concentrations is ~1 nM. The $[MK_{red}]/[MK_{ox}]$ values that yield concentrations within these limits for all four metabolites and over relatively wide ranges of $[SO_4^{2-}]_{out}$ and $[H_2S]_{in}$ depend on the kinetic parameters of the enzymes involved in the metabolic pathway. For *D. vulgaris* enzyme kinetics (Table S2) the range is between ~60 and 140 and we pick a default value of 100 for $[MK_{red}]/[MK_{ox}]$ for fitting the *D. vulgaris* data and for the model sulfate reducer. The intracellular metabolite concentrations using this value and over a range of $[SO_4^{2-}]_{out}$ and $[H_2S]_{in}$ are shown in Fig. 2 in the main text. For *A. fulgidus* enzyme kinetics, which are ~3–10 times slower than those of *D. vulgaris* (Table S2), the default value of $[MK_{red}]/[MK_{ox}]$ yielding metabolite concentrations within the physiological constraints is 40.

We note that the different redox potentials of other electron carrier pairs [e.g., reduced and oxidized cytochromec_3 (12)] would require a different ratio of reduced to oxidized electron carrier concentrations to satisfy the constraints on intracellular metabolite concentrations. Different electron carrier redox ratios and different reaction stoichiometry would also be required if electron bifurcation supports sulfate reduction [e.g., through reduced and oxidized DsrC (13)]. With the ratio of reduced to oxidized electron carrier concentrations as a free parameter, we are essentially quantifying the thermodynamic consequences of electron transfer for successful sulfate reduction. Our approach can be adapted to the exact identity of the electron carrier pair, as long as the physiological constraints on intracellular metabolite concentrations are met.

The value of the sulfate uptake kinetic fractionation factor ($^{34}\alpha_A^{kin}$) is poorly constrained and strongly controls the $^{34}\varepsilon$–$^{33}\lambda$ relationship of the full metabolic network (Fig. 5 in main text). We use experimentally observed $^{34}\varepsilon$–$^{33}\lambda$ relationships to constrain the value of $^{34}\alpha_A^{kin}$, which we allow to be strain specific. For recently published datasets (14–18), the best-fit values of $^{34}\alpha_A^{kin}$ are 0.997 and 0.993, respectively. These values are consistent with early experiments, which assign a value of −3‰ to the fractionation associated with sulfate uptake (19). For lack of experimental constraints, we use a value of 0.5146 for $^{33}\lambda$, calculated using the Swain–Schaad formalism (20). In calculations other than strain-specific fits to experimental data (model sulfate reducer and sensitivity analyses), we use default values of 0.993 and 0.5146 for $^{34}\alpha_A^{kin}$ and $^{33}\lambda$, respectively.

With $[MK_{red}]/[MK_{ox}]$, $^{34}\alpha_A^{kin}$, and $^{33}\lambda$ constrained, and with $[SO_4^{2-}]_{out}$ and $[H_2S]_{in}$ as free model parameters (to be specified for individual experimental or environmental conditions), we use the last remaining tunable parameter, $u_{vivo-vitro}$ to fit experimental $[SO_4^{2-}]_{out}$–csSRR–$^{34}\varepsilon$ data (14–17, 21, 22). The extracellular sulfate and sulfide concentrations are reported for these experiments and the latter must be related to the model parameter $[H_2S]_{in}$. Where extracellular concentrations of sulfide are not reported (e.g., in N_2-sparged experiments), we prescribe $[H_2S]_{in}$ to be 0.1 mM. As suggested by sulfide accumulation experiments (23), membrane resistance to H_2S, although very low, may be enough to enable the buildup of intracellular H_2S even when environmental sulfide levels are small. Where csSRR values were not reported for some of the data in a set of experiments (21, 22), we assigned to those data the harmonic mean of the csSRRs that were reported from that dataset.

We found that the value of $u_{vivo-vitro}$ required to fit the data of all three experimental studies depends linearly on the csSRR in the specific experiment (Fig. S2). This can be understood as the up-regulation of enzyme levels to achieve a given increase in csSRR. We used the coefficients of a least-squares linear fit to the $u_{vivo-vitro}$–csSRR data (Fig. S2 and Table S4) to calculate csSRR-dependent $u_{vivo-vitro}$ values for the model fits to the experimental data (black curves in Fig. 3 *A*, *E*, and *H* in main text).

Model Sensitivity Analysis. We tested the sensitivity of the model to the values of tunable parameters. The $^{34}\varepsilon$–csSRR and $^{34}\varepsilon - [SO_4^{2-}]_{out}$ relationships are modestly sensitive to intracellular H_2S concentrations and extremely sensitive to the ratio of oxidized to reduced electron carriers (Fig. 4 in main text). The $^{33}\lambda$–$^{34}\varepsilon$ relationship is also sensitive to these intracellular concentrations (Fig. 5 in main

text). Additionally, this relationship is sensitive to the value chosen for the kinetic fractionation associated with sulfate uptake into the cell ($^{34}\alpha_A^{kin}$; Fig. 5 in main text) and with reduction of APS ($^{34}\alpha_C^{kin}$; Fig. S3). The latter of these fractionation factors is experimentally constrained (24) and the sensitivity displayed is important for understanding limitations on sulfate reduction rate, but not for the explanation of actual isotopic variability. These sensitivities are discussed fully in the main text. In addition to these, the results are insensitive to modestly sensitive to a number of other parameter values (Fig. S3), but not in a way that qualitatively changes the results of the model or its ability to explain experimental $[SO_4^{2-}]_{out}$–csSRR–$^{34}\varepsilon$–$^{33}\lambda$ data.

1. Flamholz A, Noor E, Bar-Even A, Liebermeister W, Milo R (2013) Glycolytic strategy as a tradeoff between energy yield and protein cost. *Proc Natl Acad Sci USA* 110(24):10039–10044.
2. O'Leary MH (1981) Carbon isotope fractionation in plants. *Phytochemistry* 20:553–567.
3. Badziong W, Thauer R (1980) Vectorial electron transport in Desulfovibrio vulgaris (Marburg) growing on hydrogen plus sulfate as sole energy source. *Arch Microbiol* 125(1-2):167–174.
4. Bradley AS, Leavitt WD, Johnston DT (2011) Revisiting the dissimilatory sulfate reduction pathway. *Geobiology* 9(5):446–457.
5. Alberty RA (2006) *Biochemical Thermodynamics: Applications of Mathematica* (Wiley, Hoboken, New Jersey).
6. Flamholz A, Noor E, Bar-Even A, Milo R (2012) eQuilibrator—the biochemical thermodynamics calculator. *Nucleic Acids Res* 40(Database issue):D770–D775.
7. Thauer RK, Jungermann K, Decker K (1977) Energy conservation in chemotrophic anaerobic bacteria. *Bacteriol Rev* 41(1):100–180.
8. Kreke B, Cypionka H (1992) Protonmotive force in freshwater sulfate-reducing bacteria, and its role in sulfate accumulation in Desulfobulbus propionicus. *Arch Microbiol* 158(3): 183–187.
9. Steuber J, Arendsen AF, Hagen WR, Kroneck PM (1995) Molecular properties of the dissimilatory sulfite reductase from Desulfovibrio desulfuricans (Essex) and comparison with the enzyme from Desulfovibrio vulgaris (Hildenborough). *Eur J Biochem* 233(3):873–879.
10. Ravcheev DA, et al. (2012) Transcriptional regulation of central carbon and energy metabolism in bacteria by redox-responsive repressor Rex. *J Bacteriol* 194(5):1145–1157.
11. Bar-Even A, Noor E, Flamholz A, Buescher JM, Milo R (2011) Hydrophobicity and charge shape cellular metabolite concentrations. *PLoS Comput Biol* 7(10):e1002166.
12. Postgate JR (1965) Recent advances in the study of the sulfate-reducing bacteria. *Bacteriol Rev* 29(4):425–441.
13. Venceslau SS, et al. (2013) Redox states of Desulfovibrio vulgaris DsrC, a key protein in dissimilatory sulfite reduction. *Biochem Biophys Res Commun* 441(4):732–736.
14. Sim MS, Bosak T, Ono S (2011) Large sulfur isotope fractionation does not require disproportionation. *Science* 333(6038):74–77.
15. Sim M, Ono S, Donovan K, Templer S, Bosak T (2011) Effect of electron donors on the fractionation of sulfur isotopes by a marine Desulfovibrio sp. *Geochim Cosmochim Acta* 75:4244–4259.
16. Sim MS, Ono S, Bosak T (2012) Effects of iron and nitrogen limitation on sulfur isotope fractionation during microbial sulfate reduction. *Appl Environ Microbiol* 78(23):8368–8376.
17. Leavitt WD, Halevy I, Bradley AS, Johnston DT (2013) Influence of sulfate reduction rates on the Phanerozoic sulfur isotope record. *Proc Natl Acad Sci USA* 110(28):11244–11249.
18. Farquhar J, et al. (2003) Multiple sulphur isotopic interpretations of biosynthetic pathways: Implications for biological signatures in the sulphur isotope record. *Geobiol* 1(1):27–36.
19. Harrison A, Thode H (1958) Mechanism of the bacterial reduction of sulphate from isotope fractionation studies. *Trans Faraday Soc* 54:84–92.
20. Swain CG, Stivers EC, Reuwer JF, Jr, Schaad LJ (1958) Use of hydrogen isotope effects to identify the attacking nucleophile in the enolization of ketones catalyzed by acetic acid1-3. *J Am Chem Soc* 80:5885–5893.
21. Habicht KS, Gade M, Thamdrup B, Berg P, Canfield DE (2002) Calibration of sulfate levels in the Archean ocean. *Science* 298(5602):2372–2374.
22. Habicht KS, Salling L, Thamdrup B, Canfield DE (2005) Effect of low sulfate concentrations on lactate oxidation and isotope fractionation during sulfate reduction by Archaeoglobus fulgidus strain Z. *Appl Environ Microbiol* 71(7):3770–3777.
23. Furusaka C (1961) Sulphate transport and metabolism by Desulphovibrio desulphuricans. *Nature* 192:427–429.
24. Kemp A, Thode H (1968) The mechanism of the bacterial reduction of sulphate and of sulphite from isotope fractionation studies. *Geochim Cosmochim Acta* 32(1):71–91.

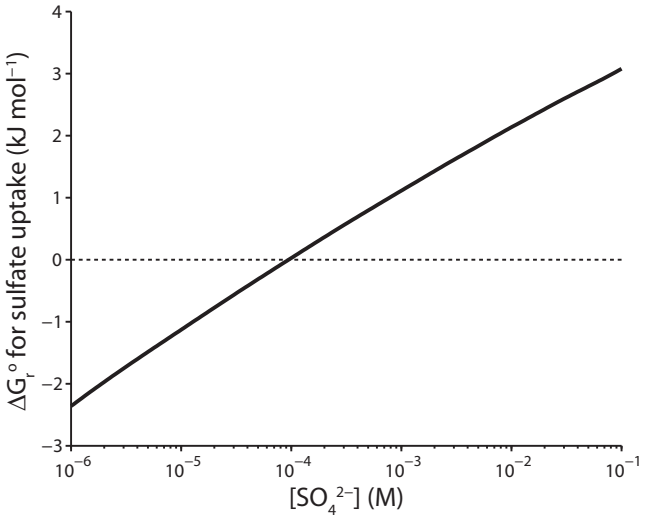

Fig. S1. Gibbs free energy of reaction at standard state for sulfate uptake as a function of extracellular sulfate concentration calculated using Eqs. **S13–S15**.

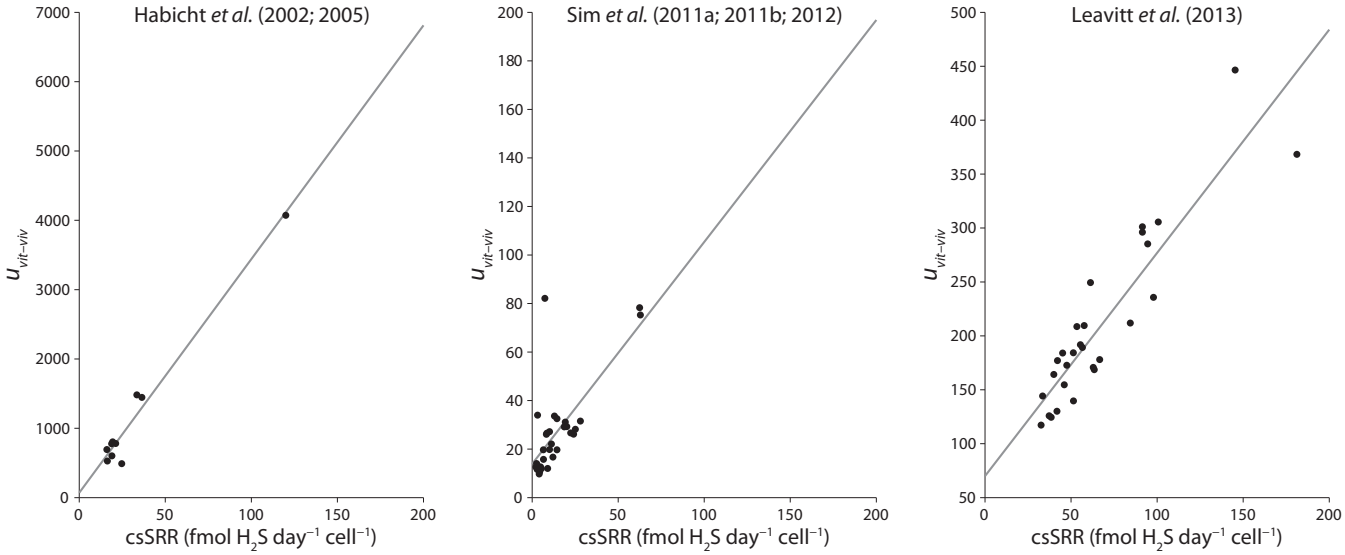

Fig. S2. The vivo–vitro scaling factor ($u_{vivo-vitro}$) required to fit $^{34}\varepsilon$–csSRR data as a function of csSRR (markers) and linear fits (lines) to the data ($R^2 = 0.97$, 0.52, and 0.82 for *Left*, *Center*, and *Right* plots, respectively).

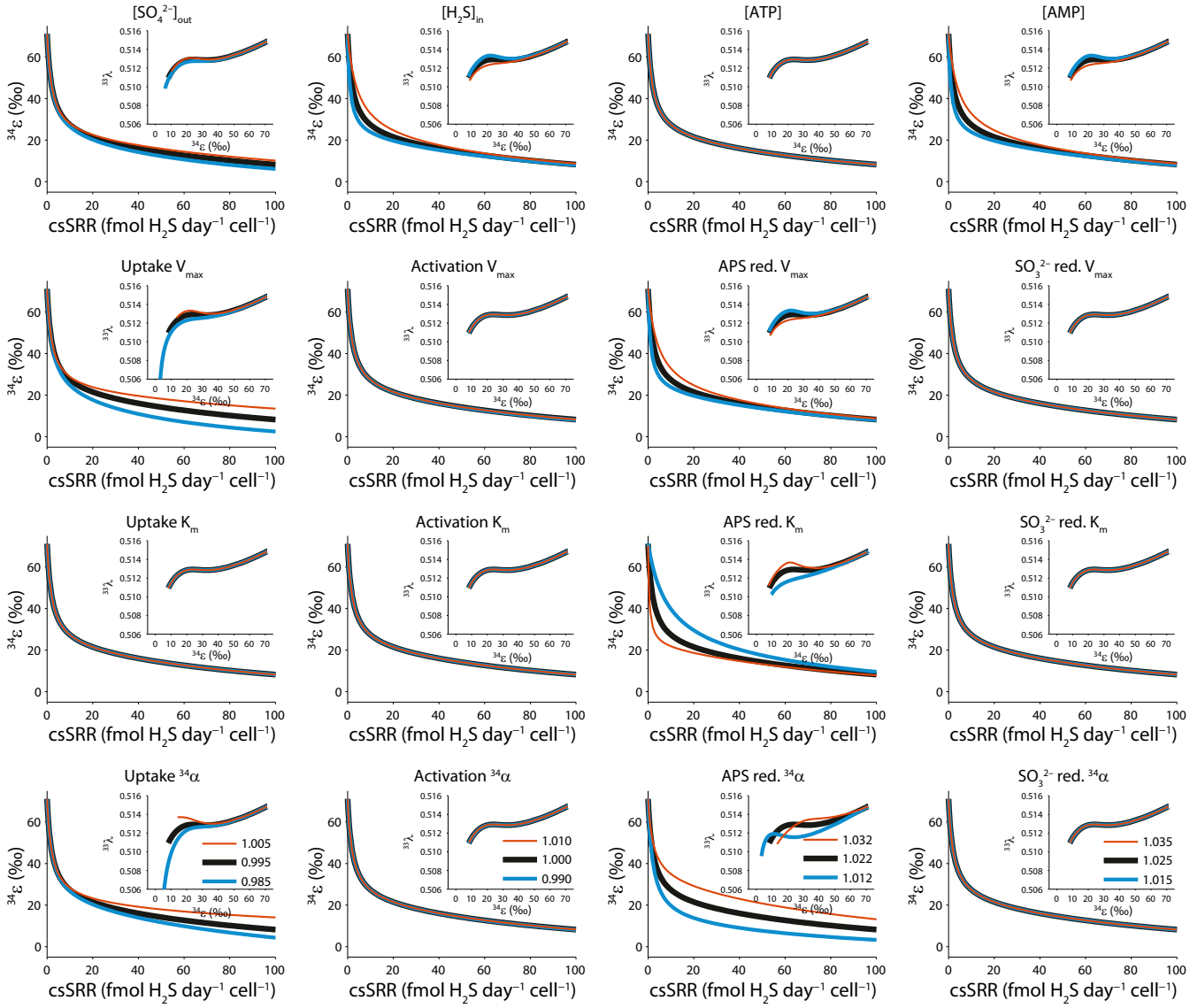

Fig. S3. Sensitivity of model results to parameter values. The main plots show the $^{34}\varepsilon$–csSRR relationships and *Insets* show the $^{33}\lambda$–$^{34}\varepsilon$ relationships. Black curves are for default parameter values (Tables S2–S4). Blue and orange curves are for half and twice the default values, respectively, except for the sensitivity analyses to the kinetic fractionation factors associated with each of the metabolic reactions (*Bottom* row), where the values of the fractionation factors are shown in *Insets*.

Table S1. Metabolic reactions for dissimilatory sulfate reduction

Step	Reaction
A	$SO^{2-}_{4\ out} + nH^{+}_{out} \rightleftharpoons SO^{2-}_{4\ in} + nH^{+}_{in}$
B	$SO^{2-}_{4\ in} + ATP \rightleftharpoons APS + PPi$
C	$APS + MK_{red} \rightleftharpoons SO^{2-}_{3} + MK_{ox} + AMP$
D	$SO^{2-}_{3} + 3MK_{red} + 2H^{+}_{in} \rightleftharpoons H_2S + 3MK_{ox} + 3H_2O$

AMP, adenosine monophosphate; ATP, adenosine triphosphate; MK_{ox}, menaquinone, oxidized; MK_{red}, menaquinone, reduced; PPi, pyrophosphate; ΔG^{o}_{A}, see Fig. S1; $\Delta G^{o'}_{B} = 55.9\ kJ \cdot mol^{-1}$; $\Delta G^{o'}_{C} = 5.4\ kJ \cdot mol^{-1}$; $\Delta G^{o'}_{D} = 31.2\ kJ \cdot mol^{-1}$.

Table S2. In vitro enzyme kinetic parameters used in the model

Step	V^+	K_m		Notes	Source or ref.
A: $SO_{4\ out}^{2-} + nH_{out}^+ \rightleftharpoons SO_{4\ in}^{2-} + nH_{in}^+$					
Archaeoglobus fulgidus	1.68×10^{-20}			Harmonic mean of all data	†
Desulfovibrio vulgaris	3.98×10^{-20}			Harmonic mean of *D. vulgaris* data	†
		SO_4^{2-}	0.01	Approximate harmonic mean of *D. vulgaris* data	†
B: $SO_{4\ in}^{2-} + ATP \rightleftharpoons APS + PPi$					
A. fulgidus	1.71×10^{-19}			Internally consistent* harmonic mean of *A. fulgidus* data	†
D. vulgaris	3.24×10^{-19}			Internally consistent* harmonic mean of *D. vulgaris* data	†
		SO_4^{2-}	10.00	Estimate based on range of reported values and $[SO_4^{2-}]$	(1)
		ATP	0.10	Estimate based on range of reported values	(1)
		APS	0.17	Estimate based on *A. fulgidus*	(1)
		PPi	0.13	Estimate based on *A. fulgidus*	(1)
C: $APS + MK_{red} \rightleftharpoons SO_3^{2-} + MK_{ox} + AMP$					
A. fulgidus	9.38×10^{-20}			Internally consistent* *A. fulgidus* data	†
D. vulgaris	3.49×10^{-19}			Internally consistent* *D. vulgaris* data	†
		APS	0.02	Estimate based on *D. vulgaris*, *A. fulgidus*	(1)
		MK_{red}	0.10	Estimate based on *Desulfobulbus propionicus*, *Desulfovibrio gigas*	(1)
		MK_{ox}	0.10	Estimate based on *D. propionicus*, *D. gigas*	(1)
		SO_3^{2-}	0.40	Estimate based on *D. vulgaris*, *Desulfovibrio salexigens*, *D. gigas*, *Desulfovibrio desulfuricans*	(1)
		AMP	0.30	Estimate based on *D. vulgaris*, *D. salexigens*, *D. desulfuricans*	(1)
D: $SO_3^{2-} + 3MK_{red} + 2H_{in}^+ \rightleftharpoons H_2S + 3MK_{ox} + 3H_2O$					
A. fulgidus	2.38×10^{-20}			Internally consistent* *A. fulgidus* data	†
D. vulgaris	4.28×10^{-19}			Internally consistent* *D. vulgaris* data	†
		SO_3^{2-}	0.05	Estimate based on reported values for *D. vulgaris*	(1)
		MK_{red}	0.02	Estimate based on range of reported values	(1)
		MK_{ox}	0.02	Estimate based on range of reported values	(1)
		H_2S	0.01	Estimate	

The values for *D. vulgaris* were also used for the model sulfate reducer and as default values in the sensitivity analyses. The units of V^+ are $mol \cdot cell^{-1} \cdot s^{-1}$. The units of K_m are mM for presentation purposes. The actual calculations require units of M.

*All values were taken from publications by the same research group to ensure similarity of methods (See Dataset S1).

†Dataset S1.

1. Schomburg I, et al. (2013) BRENDA in 2013: Integrated reactions, kinetic data, enzyme function data, improved disease classification: New options and contents in BRENDA. *Nucleic Acids Res* 41(Database issue):D764–D772.

Table S3. Equilibrium and kinetic fractionation factors and mass-dependent exponents used in the model

Step	$^{34}\alpha^{eq}$	$^{33}\lambda^{eq}$	Ref.	$^{34}\alpha^{kin}$	$^{33}\lambda^{kin}$*	Ref.
T = 25 °C, for *D. vulgaris* experiments						
A	1.000	0.5150	(1)	0.993–0.997†	0.5146	(2)
B	1.000	0.5150	(1)	1.000	0.5146	NA
C	1.006	0.5167	(1)	1.022	0.5146	(3)
D	1.065	0.5147	(1)	1.025	0.5146	(4)
T = 80 °C, for *A. fulgidus* experiments						
A	1.000	0.5150	(1)	0.993–0.997†	0.5146	(2)
B	1.000	0.5150	(1)	1.000	0.5146	NA
C	1.004	0.5165	(1)	1.022	0.5146	(3)
D	1.050	0.5149	(1)	1.025	0.5146	(4)

*The fractionation exponent was calculated with the Swain–Schaad formalism (5), where $^{33}\alpha^{kin} = \left(^{34}\alpha^{kin}\right)^{^{33}\lambda^{kin}}$.
†The upper end of this range (0.997) was suggested by Harrison and Thode (2) and required to adequately fit the $^{33}\lambda$–$^{34}\varepsilon$ datasets of Sim et al. (6–8). The lower end (0.993) was required to adequately fit the $^{33}\lambda$–$^{34}\varepsilon$ datasets of Habicht et al. (9, 10) and Leavitt et al. (11).

1. Otake T, Lasaga AC, Ohmoto H (2008) Ab initio calculations for equilibrium fractionations in multiple sulfur isotope systems. *Chem Geol* 249:357–376.
2. Harrison A, Thode H (1958) Mechanism of the bacterial reduction of sulphate from isotope fractionation studies. *Trans Faraday Soc* 54:84–92.
3. Kemp A, Thode H (1968) The mechanism of the bacterial reduction of sulphate and of sulphite from isotope fractionation studies. *Geochim Cosmochim Acta* 32(1):71–91.
4. Hoek J, Canfield D (2009) Controls on isotope fractionation during sulfate reduction. *Geochim Cosmochim Acta* 73:A538.
5. Swain CG, Stivers EC, Reuwer JF, Jr, Schaad LJ (1958) Use of hydrogen isotope effects to identify the attacking nucleophile in the enolization of ketones catalyzed by acetic acid1-3. *J Am Chem Soc* 80:5885–5893.
6. Sim MS, Bosak T, Ono S (2011) Large sulfur isotope fractionation does not require disproportionation. *Science* 333(6038):74–77.
7. Sim M, Ono S, Donovan K, Templer S, Bosak T (2011) Effect of electron donors on the fractionation of sulfur isotopes by a marine Desulfovibrio sp. *Geochim Cosmochim Acta* 75:4244–4259.
8. Sim MS, Ono S, Bosak T (2012) Effects of iron and nitrogen limitation on sulfur isotope fractionation during microbial sulfate reduction. *Appl Environ Microbiol* 78(23):8368–8376.
9. Habicht KS, Gade M, Thamdrup B, Berg P, Canfield DE (2002) Calibration of sulfate levels in the archean ocean. *Science* 298(5602):2372–2374.
10. Habicht KS, Salling L, Thamdrup B, Canfield DE (2005) Effect of low sulfate concentrations on lactate oxidation and isotope fractionation during sulfate reduction by Archaeoglobus fulgidus strain Z. *Appl Environ Microbiol* 71(7):3770–3777.
11. Leavitt WD, Halevy I, Bradley AS, Johnston DT (2013) Influence of sulfate reduction rates on the Phanerozoic sulfur isotope record. *Proc Natl Acad Sci USA* 110(28):11244–11249.

Table S4. Parameter values used in the model

Parameter	Value	Source or ref.	Notes
[ATP]	2.6 mM	(1, 2)	For *D. vulgaris*
[AMP]	0.3 mM	(1)	For *D. vulgaris*
[MK]	0.6 mM	(3)	For *D. vulgaris* Marburg
$[MK_{red}]/[MK_{ox}]$	100 or 40*	This study	See *Model Calibration*
$u_{vivo-vitro}$			
Model sulfate reducer	2.0 × csSRR + 70.0†	This study	
Habicht et al. (4, 5)	33.7 × csSRR + 70.1	This study	See Fig. S2
Sim et al. (6–8)	0.9 × csSRR + 13.9	This study	See Fig. S2
Leavitt et al. (9)	2.1 × csSRR + 70.0	This study	See Fig. S2

*$[MK_{red}]/[MK_{ox}]$ of 100 was used for the model sulfate reducer, for the fits to the *D. vulgaris* data (6–9), and for the sensitivity analyses. $[MK_{red}]/[MK_{ox}]$ of 40 was used for the fit to the *A. fulgidus* data (4, 5).
†The linear relationship between csSRR and $u_{vivo-vitro}$ in the model sulfate reducer was based on the fit to the data of Leavitt et al. (9).

1. Yagi T, Ogata M (1996) Catalytic properties of adenylylsulfate reductase from Desulfovibrio vulgaris Miyazaki. *Biochimie* 78(10):838–846.
2. Sekiguchi T, Noguchi A, Nosoh Y (1977) ATP and acetylene-reducing activity of a sulfate-reducing bacterium. *Can J Microbiol* 23(5):567–572.
3. Badziong W, Thauer R (1980) Vectorial electron transport in Desulfovibrio vulgaris (Marburg) growing on hydrogen plus sulfate as sole energy source. *Arch Microbiol* 125:167–174.
4. Habicht KS, Gade M, Thamdrup B, Berg P, Canfield DE (2002) Calibration of sulfate levels in the archean ocean. *Science* 298(5602):2372–2374.
5. Habicht KS, Salling L, Thamdrup B, Canfield DE (2005) Effect of low sulfate concentrations on lactate oxidation and isotope fractionation during sulfate reduction by Archaeoglobus fulgidus strain Z. *Appl Environ Microbiol* 71(7):3770–3777.
6. Sim MS, Bosak T, Ono S (2011) Large sulfur isotope fractionation does not require disproportionation. *Science* 333(6038):74–77.
7. Sim M, Ono S, Donovan K, Templer S, Bosak T (2011) Effect of electron donors on the fractionation of sulfur isotopes by a marine Desulfovibrio sp. *Geochim Cosmochim Acta* 75:4244–4259.
8. Sim MS, Ono S, Bosak T (2012) Effects of iron and nitrogen limitation on sulfur isotope fractionation during microbial sulfate reduction. *Appl Environ Microbiol* 78(23):8368–8376.
9. Leavitt WD, Halevy I, Bradley AS, Johnston DT (2013) Influence of sulfate reduction rates on the Phanerozoic sulfur isotope record. *Proc Natl Acad Sci USA* 110(28):11244–11249.

Other Supporting Information Files

Dataset S1 (XLSX)